

## Article

# Preparation of Activated Biochar-Supported Magnetite Composite for Adsorption of Polychlorinated Phenols from Aqueous Solutions

Byung-Moon Jun <sup>1,†</sup>, Yejin Kim <sup>2,†</sup>, Jonghun Han <sup>3</sup>, Yeomin Yoon <sup>1</sup>, Jeonggwon Kim <sup>4,\*</sup> and Chang Min Park <sup>2,\*</sup>

<sup>1</sup> Department of Civil and Environmental Engineering, University of South Carolina, Columbia, 300 Main Street, SC 29208, USA

<sup>2</sup> Department of Environmental Engineering, Kyungpook National University, 80 Daehak-ro, Buk-gu, Daegu 41566, Korea

<sup>3</sup> Department of Civil and Environmental Engineering, Korea Army Academy at Yeongcheon, 495 Hogook-ro, Gokyeungmeon, Yeongcheon, Gyeongbuk 38900, Korea

<sup>4</sup> Korea Environmental Industry & Technology Institute, 215 Jinheungno, Eunpyeong-gu, Seoul 03367, Korea

\* Correspondence: jgwan@keiti.re.kr (J.K.); cmpark@knu.ac.kr (C.M.Park); Tel.: +82-10-5303-7831 (J.K.); +82-53-950-6581 (C.M.P.)

<sup>†</sup> The first two authors contributed equally.

Received: 20 July 2019; Accepted: 9 September 2019; Published: 11 September 2019

**Abstract:** For this study, we applied activated biochar (AB) and its composition with magnetite (AB-Fe<sub>3</sub>O<sub>4</sub>) as adsorbents for the removal of polychlorophenols in model wastewater. We comprehensively characterized these adsorbents and performed adsorption tests under several experimental parameters. Using FTIR, we confirmed successful synthesis of AB-Fe<sub>3</sub>O<sub>4</sub> composite through cetrimonium bromide surfactant. We conducted adsorption tests using AB and AB-Fe<sub>3</sub>O<sub>4</sub> to treat model wastewater containing polychlorophenols, such as 2,3,4,6-Tetrachlorophenol (TeCP), 2,4,6-Trichlorophenol (TCP), and 2,4-Dichlorophenol (DCP). Results of the isotherm and the kinetic experiments were well adapted to Freundlich's isotherm model and the pseudo-second-order kinetic model, respectively. Main adsorption mechanisms in this study were attributed to non-covalent,  $\pi$ -electron acceptor–donor interactions and hydrophobic interactions judging from the number of chloride elements in each chlorophenol and its hydrophobic characteristics. We also considered the electrostatic repulsion effect between TeCP and AB, because adsorption performance of TeCP at basic condition was slightly worse than at weak acidic condition. Lastly, AB-Fe<sub>3</sub>O<sub>4</sub> showed high adsorption selectivity of TeCP compared to other persistent organic pollutants (i.e., bisphenol A and sulfamethoxazole) due to hydrophobic interactions. We concluded that AB-Fe<sub>3</sub>O<sub>4</sub> may be used as novel adsorbent for wastewater treatment including toxic and hydrophobic organic pollutants (e.g., TeCP).

**Keywords:** biochar activation; AB-Fe<sub>3</sub>O<sub>4</sub>; polychlorophenols; wastewater

## 1. Introduction

In the past decades, several efficient ways to treat wastewater containing organic and inorganic pollutants have been considered as one of the important topics in environmental science [1–5]. Chlorinated organic compounds (e.g., dioxins, polychlorophenols) are known as significant environmental pollutants, because these compounds have great resistance to biological degradation processes and affect serious health problems (e.g., nervous or respiratory systems) via the bioaccumulation of organisms in the ecosystem [6]. The emission of chlorinated organic compounds

could be a result of combustion processes or several industries such as pulp, herbicides, petroleum refineries, dyes, pharmaceuticals, and pesticides [7,8]. Particularly, polychlorophenols have been regulated as toxic pollutants by the U.S. Environmental Protection Agency due to its carcinogenic properties [7], thus it is crucial to investigate the effective way for removal of polychlorophenols from aqueous phase.

The various physico-chemical or biological methods that have previously been proposed to treat chlorophenols in wastewater are as follows: adsorption [9], incineration [7], photodegradation [10], electrochemical oxidation [11], catalytic degradation [12], biodegradation [13], and using a hybrid bioreactor [14]. However, secondary pollution could be generated by toxic byproducts in chemical treatments [15]. Furthermore, high operational costs and low efficiency have been described as weaknesses of biological treatments [7]. Thus, the adsorption process could be considered as an efficient method due to its simplicity, accessibility, cost-effectiveness, and high removal efficiency with reusability [16–20]. Novel adsorbents are essential for increasing removal efficiency of adsorbates in the adsorption process, and several adsorbents have been utilized to treat chlorophenols through carbon nanotubes, graphene oxides, activated carbon fibers, biochars, natural clays, and minerals [9,11,12].

Biochar is a kind of pyrogenic carbon material obtained from the combustion of biomass via pyrolysis [21]. This low-cost material has attracted attention since it can be used as an efficient adsorbent to remove organic pollutants with its outstanding adsorption physico-chemical properties. In other words, high adsorption efficiency of biochar can be attributed to its high porosity, large surface area, great ion-exchange capacity, and tunable surface chemistry [21,22]. For instance, biochar has been used as an effective adsorbent for treatment of wastewater that contains several toxic organic and inorganic pollutants such as phenol, dyes, chlorophenols, heavy metals, and pharmaceuticals [23]. Although raw biochar is applicable in many situations as an adsorbent, adsorption properties may be enhanced with further activation using various acids (e.g., HCl, HNO<sub>3</sub>, H<sub>2</sub>SO<sub>4</sub>, and H<sub>3</sub>PO<sub>4</sub>) [23]. In other words, physico-chemical properties can be modified by modifying parameters, thus the pore size or the chemical bonds of biochar can change with activation agents and exposure time [24]. For example, the physical properties of biochar were improved by HCl activation, as revealed by an increased surface area from 289 to 347 m<sup>2</sup>/g [23]. In addition, increased oxygenated functional groups after activation (e.g., carboxyl, hydroxyl, and carbonyl groups) could have positive or negative effects depending on the chemical structure of adsorbates [25].

Nanocomposite materials—iron-based magnetic nanoparticles, in particular (e.g., Fe<sub>2</sub>O<sub>3</sub> and Fe<sub>3</sub>O<sub>4</sub>)—and their efficiency in removing toxic pollutants from wastewater have been widely studied [26]. Magnetite is generally produced by co-precipitation using Fe(II)/Fe(III) salts under anaerobic condition, and performances of synthesized magnetite are attributed to preparation parameters such as solution pH, temperature, and co-ions [27]. Magnetite has been used for composite materials to treat toxic pollutants in wastewater using its high surface area, reusability by external magnetic field, reproducibility, mechanical property, and adsorption ability [28]. Thus, there is synergetic effect if magnetite is synthesized with activated biochar (AB) as a novel adsorbent according to previous studies [9,27,28]. To the best of our knowledge, our study was the first attempt to treat 2,3,4,6-Tetrachlorophenol (TeCP), 2,4,6-Trichlorophenol (TCP), and 2,4-Dichlorophenol (DCP) in model wastewater via AB-Fe<sub>3</sub>O<sub>4</sub>.

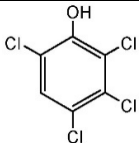
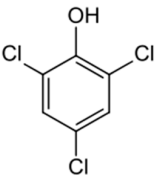
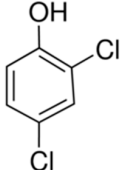
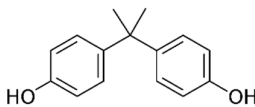
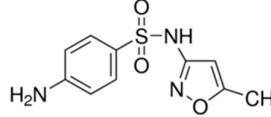
The main goal of this study was to evaluate the feasibility of AB-Fe<sub>3</sub>O<sub>4</sub> as an adsorbent to remove selected polychlorophenols. We first conducted several characterizations in order to evaluate the physico-chemical properties of synthesized AB-Fe<sub>3</sub>O<sub>4</sub>. Subsequently, we carried out the adsorption process of polychlorophenols under the following experimental parameters: contact time for kinetics, initial concentration of polychlorophenols for isotherms, and solution pH. Lastly, we measured adsorption selectivity of TeCP by AB-Fe<sub>3</sub>O<sub>4</sub> compared to other persistent organic pollutants [i.e., bisphenol A (BPA) and sulfamethoxazole (SMX)].

## 2. Materials and Methods

### 2.1. Materials

We purchased commercially available nitric acid (HNO<sub>3</sub>), sulfuric acid (H<sub>2</sub>SO<sub>4</sub>), sodium hydroxide (NaOH), ferrous chloride (FeCl<sub>2</sub>·4H<sub>2</sub>O), ferric chloride (FeCl<sub>3</sub>·6H<sub>2</sub>O), BPA (C<sub>15</sub>H<sub>16</sub>O<sub>2</sub>), SMX (C<sub>10</sub>H<sub>11</sub>N<sub>3</sub>O<sub>3</sub>S), 2,3,4,6-TeCP (C<sub>6</sub>H<sub>2</sub>Cl<sub>4</sub>O), 2,4,6-TCP (C<sub>6</sub>H<sub>3</sub>Cl<sub>3</sub>O), 2,4-DCP (C<sub>6</sub>H<sub>4</sub>Cl<sub>2</sub>O), methanol (CH<sub>4</sub>O), and cetrimonium bromide (CTAB, C<sub>19</sub>H<sub>42</sub>BrN) from Sigma-Aldrich (St. Louis, MO, USA). Table 1 summarizes selected physicochemical properties of TeCP, TCP, DCP, BPA, and SMX. Stock and feed solutions were prepared using deionized (DI) water.

**Table 1.** Selected physicochemical properties of 2,3,4,6-Tetrachlorophenol (TeCP), 2,4,6-Trichlorophenol (TCP), 2,4-Dichlorophenol (DCP), bisphenol A (BPA), and sulfamethoxazole (SMX).

Compound [Full name]	Formula	MW (g/mol)	pK <sub>a</sub>	Water solubility (M)	log K <sub>ow</sub>	Molecular structure
2,3,4,6-Tetrachlorophenol	C <sub>6</sub> H <sub>2</sub> Cl <sub>4</sub> O	231.9	5.22	9.92 × 10 <sup>−5</sup>	4.45	
2,4,6-Trichlorophenol	C <sub>6</sub> H <sub>3</sub> Cl <sub>3</sub> O	197.4	6.23	2.78 × 10 <sup>−2</sup>	3.69	
2,4-Dichlorophenol	C <sub>6</sub> H <sub>4</sub> Cl <sub>2</sub> O	162.9	7.89	3.01 × 10 <sup>−2</sup>	3.06	
Bisphenol A [2,2-bis(4-hydroxyphenyl) propane; 4,4'-dihydroxy- 2,2-diphenylpropane]	C <sub>15</sub> H <sub>16</sub> O <sub>2</sub>	228.3	9.6	5.26 × 10 <sup>−4</sup>	3.32	
Sulfamethoxazole [4-amino-N-(5-methyl-1,2- oxazol-3-yl) benzenesulfonamide]	C <sub>10</sub> H <sub>11</sub> N <sub>3</sub> O <sub>3</sub> S	253.3	1.6, 5.7	3.21 × 10 <sup>−2</sup> (37°C)	0.89	

## 2.2. Fabrication of AB, Fe<sub>3</sub>O<sub>4</sub>, and AB-Fe<sub>3</sub>O<sub>4</sub>

Bamboo particles as biomass feedstock were carbonized by being heated in a tubular furnace for 1.5 h at 773 K under an argon atmosphere. The carbonized material (biochar) was then left to cool in argon until 298 K, ground, and sieved to −200 mesh. Subsequently, we activated 5 g of biochar via an acid treatment using H<sub>2</sub>SO<sub>4</sub>/HNO<sub>3</sub> mixture [3:1 (v/v)] at 353 K for 3 h, as suggested in a previous study [29]. AB was then washed several times with DI to remove residual acids, and the clean AB was collected through centrifugation.

The magnetite (Fe<sub>3</sub>O<sub>4</sub>) particles were produced using a co-precipitation method based on a previous report [30]. We prepared a solution (50 mL) containing FeCl<sub>2</sub>·4H<sub>2</sub>O (2.0 g) and FeCl<sub>3</sub>·6H<sub>2</sub>O (5.2 g) dissolved in 1 M HCl (1 mL) under a nitrogen atmosphere. Then, 1 M NaOH was added dropwise into the mixture solution with vigorous stirring for 3 h. Then, fabricated Fe<sub>3</sub>O<sub>4</sub> particles were collected by an external magnetic field, washed several times using DI water, and then dried in a vacuum oven.

The synthesis of AB-Fe<sub>3</sub>O<sub>4</sub> was prepared as follows: 5 g of AB was dispersed into a beaker including 100 mL DI water through a magnetic stirrer. Then, 0.1% CTAB surfactant (w/w) was added to the beaker and stirred for 30 min to produce AB-CTAB complexation. The long chain cationic

surfactant (CTAB) intercalated to AB-Fe<sub>3</sub>O<sub>4</sub> converted the surface property to a more hydrophobic characteristic, which helped increase the adsorption of polychlorophenols [31,32]. Lastly, we mixed Fe<sub>3</sub>O<sub>4</sub> (2.5 g) with AB-CTAB complexation and stirred vigorously for 60 min. The final AB-Fe<sub>3</sub>O<sub>4</sub> products were washed several times with DI water and then separated by vacuum filtration. The cleaned products were kept in a vacuum oven until we conducted the adsorption experiments.

### 2.3. Characterization Methods

Physico-chemical properties of adsorbents were investigated by various characterization techniques. We analyzed the crystalline structure of biochar, AB, Fe<sub>3</sub>O<sub>4</sub>, and AB-Fe<sub>3</sub>O<sub>4</sub> via powder X-ray diffraction (PXRD, D/max-2500; Rigaku, Tokyo, Japan). Analyses of PXRD peaks were carried out using well-known references (Jade software; Materials Data, Inc., Livermore, CA, USA). Chemical properties of biochar, AB, Fe<sub>3</sub>O<sub>4</sub>, and AB-Fe<sub>3</sub>O<sub>4</sub> were analyzed via Fourier-transform infrared spectroscopy (FTIR; Thermo Nicolet; Madison, WI, USA) in order to identify each chemical bond [33]. The surface morphology of AB, Fe<sub>3</sub>O<sub>4</sub>, and AB-Fe<sub>3</sub>O<sub>4</sub> was analyzed using scanning electron microscopy with energy-dispersive x-ray spectroscopy (SEM-EDX, S-4200; Hitachi, Tokyo, Japan). The surface charge of 100 mg/L AB, Fe<sub>3</sub>O<sub>4</sub>, and AB-Fe<sub>3</sub>O<sub>4</sub> was obtained via zeta potential analyzer (Nano ZS; Malvern Instruments Ltd., Malvern, UK) at pH 3.5, 7, and 10 adjusted by 0.1 M HNO<sub>3</sub> and NaOH. The magnetic hysteresis loops of Fe<sub>3</sub>O<sub>4</sub> and AB-Fe<sub>3</sub>O<sub>4</sub> were evaluated via a vibrating sample magnetometer (VSM, 7407-S; Lake Shore Cryotronics, OH, USA) at room temperature. Textural characteristics of AB, Fe<sub>3</sub>O<sub>4</sub>, and AB-Fe<sub>3</sub>O<sub>4</sub> were confirmed by porosimeter (Quadrasorb SI; Quantachrome Instruments Ltd., FL, USA).

### 2.4. Adsorption Experiments

In this work, we aimed to measure the efficiency of polychlorophenols adsorption by a prepared adsorbent (AB-Fe<sub>3</sub>O<sub>4</sub>). Feed solutions including polychlorophenols (TeCP, TCP, and DCP) or pharmaceuticals (BPA and SMX) were diluted from 100 mg/L methanol-based stock solutions. Adsorption tests were conducted in a 60 mL polyethylene plastic bottle containing 30 mg of adsorbent mass and 30 mL of total liquid volume. Kinetic and isotherm adsorption studies were carried out at different exposure times (i.e., 15, 30, 45, 60, 120, and 240 min) and initial concentrations of adsorbates (i.e., 5, 10, 20, 60, 100, and 200 mg/L). Solution pH was adjusted by 0.1 M HNO<sub>3</sub> and NaOH before adsorption tests. The concentration of filtered samples was measured by high-performance liquid chromatography (1200 series; Agilent Technologies, Inc., Santa Clara, CA, USA).

### 2.5. Data Analysis

Adsorption performances of TeCP by AB and AB-Fe<sub>3</sub>O<sub>4</sub> were evaluated through adsorption capacity at equilibrium state ( $q_e$ , mg/g), as shown in Equation (1):

$$q_e = \frac{(C_0 - C_e) V}{m} \quad (1)$$

where  $C_0$  (mg/L) is the initial concentration of TeCP,  $C_e$  (mg/L) is the concentration of TeCP at equilibrium state,  $V$  (L) is the volume of the total solution containing TeCP and each adsorbent, and  $m$  (g) is mass of each adsorbent.

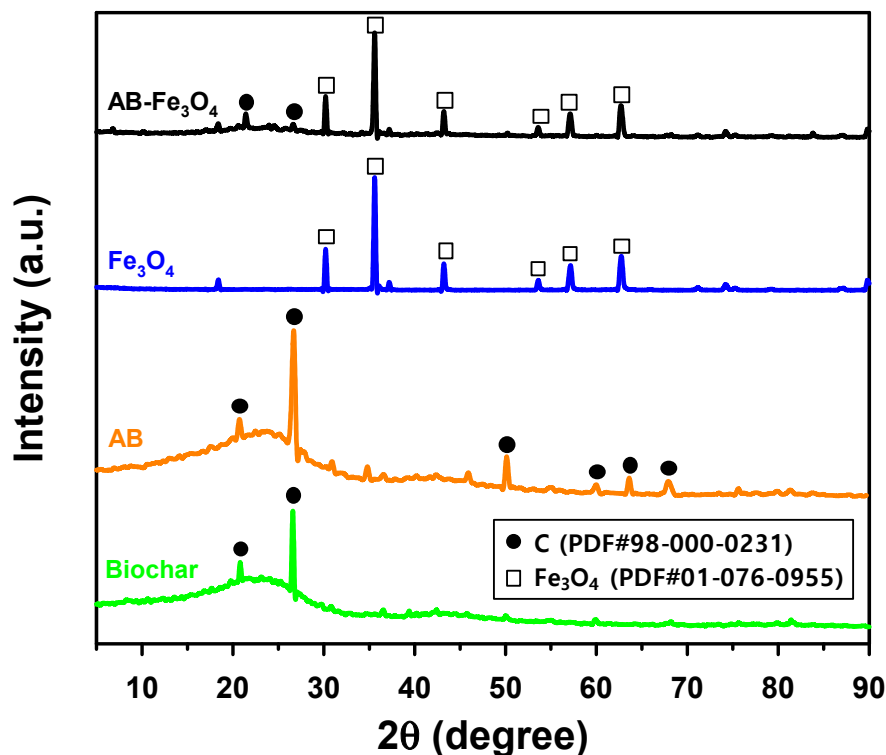
We referenced another study to conduct kinetic and isotherm experiments on target compounds' adsorption on adsorbents [15]. We used pseudo-first-order and pseudo-second-order kinetic models to investigate kinetic study of adsorption on adsorbents and applied Langmuir and Freundlich isotherm models to verify the isotherm adsorption mechanism in this system.

## 3. Results and Discussion

### 3.1. Characterizations of Biochar, AB, Fe<sub>3</sub>O<sub>4</sub>, and AB-Fe<sub>3</sub>O<sub>4</sub>

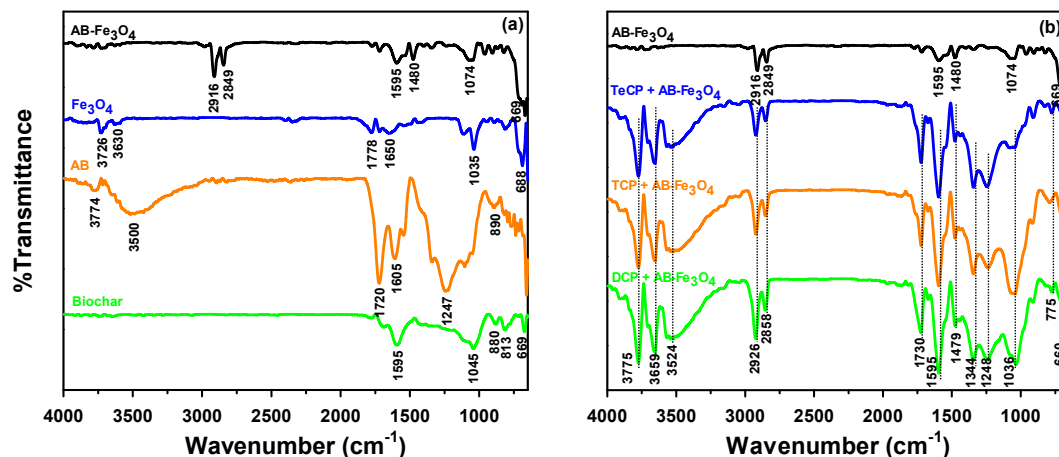
The crystalline structures of biochar, AB, Fe<sub>3</sub>O<sub>4</sub>, and AB-Fe<sub>3</sub>O<sub>4</sub> were analyzed by PXRD, which are summarized in Figure 1. The PXRD pattern of Fe<sub>3</sub>O<sub>4</sub> was comparable to another study [34], and

both  $\text{Fe}_3\text{O}_4$  and AB patterns were overlapped in a PXRD pattern of AB- $\text{Fe}_3\text{O}_4$  composite, indicating successful synthesis of AB- $\text{Fe}_3\text{O}_4$  composite.



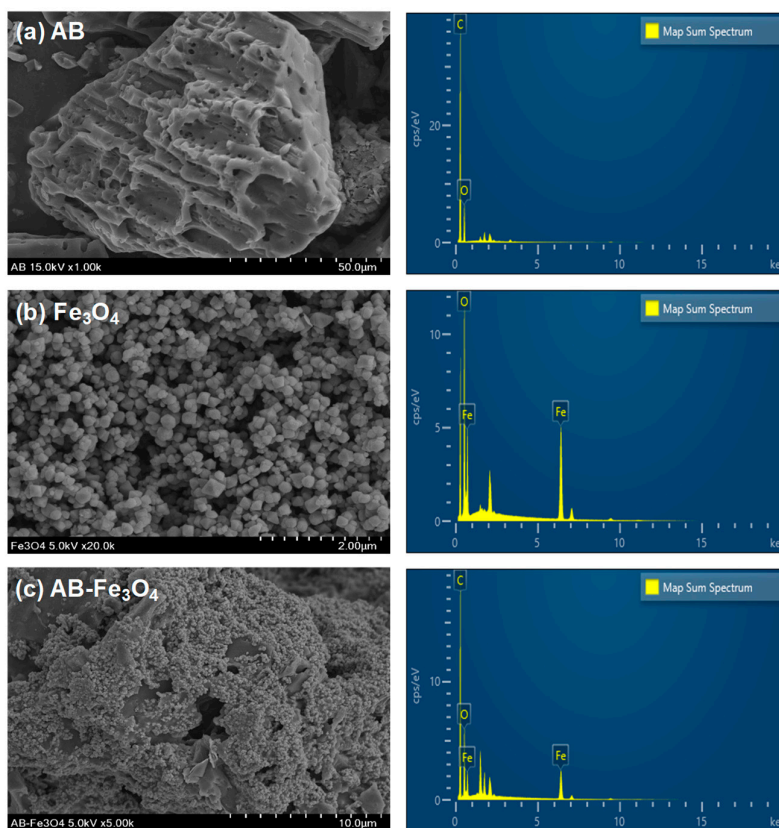
**Figure 1.** Powder X-ray diffraction (PXRD) patterns of biochar, activated biochar (AB),  $\text{Fe}_3\text{O}_4$ , and AB- $\text{Fe}_3\text{O}_4$ .

In terms of chemical bonds, we analyzed the FTIR spectra of biochar, AB,  $\text{Fe}_3\text{O}_4$ , and AB- $\text{Fe}_3\text{O}_4$  (Figure 2a). New peaks appeared after activation via acid treatments when AB (orange line in Figure 2a) was compared to biochar (green line in Figure 2a). We attributed these peaks to oxygenated functional groups [e.g., carboxyl ( $1720\text{ cm}^{-1}$ ) and hydroxyl ( $3500$  and  $1247\text{ cm}^{-1}$ )] judging from the results of other studies [29,35]. The newly formed peaks of AB- $\text{Fe}_3\text{O}_4$  (black line in Figure 2a) at  $2916$  and  $2849\text{ cm}^{-1}$  represented methyl ( $2916\text{ cm}^{-1}$ ) and methylene ( $2849\text{ cm}^{-1}$ ) functional groups of CTAB surfactant, which was used for synthesis of AB- $\text{Fe}_3\text{O}_4$  [31]. Thus, FTIR spectra of AB- $\text{Fe}_3\text{O}_4$  (black line in Figure 2a) showed successful synthesis as a composite material based on overlapping peaks of  $\text{Fe}_3\text{O}_4$  ( $1035\text{ cm}^{-1}$  of blue line in Figure 2a) and AB ( $1605\text{ cm}^{-1}$  of orange line in Figure 2a), respectively. Furthermore, we conducted the further analyses of FTIR to clarify the change of chemical bonds before and after adsorption of TeCP, TCP, and DCP on AB- $\text{Fe}_3\text{O}_4$ , as shown in Figure 2b. According to Figure 2b, FTIR spectra were evidently changed after TeCP, TCP, and DCP adsorption on AB- $\text{Fe}_3\text{O}_4$ . First of all, new peaks at  $3775$ ,  $3659$ , and  $3524\text{ cm}^{-1}$  were detected after adsorption, and these peaks could have resulted from hydroxyl group of chlorophenols [36]. Secondly, the  $\text{C}=\text{C}$  stretching vibration of AB- $\text{Fe}_3\text{O}_4$  at  $1480\text{ cm}^{-1}$  was slightly shifted to a lower wave number, which could be explained by  $\pi-\pi$  interaction between adsorbent and adsorbates [37]. Lastly, the  $\text{C}-\text{Cl}$  stretching vibration of chlorophenols in the range from  $800$  to  $600\text{ cm}^{-1}$  (i.e.,  $775\text{ cm}^{-1}$  in this study) was detected after TeCP, TCP, and DCP adsorption [38]. These results indicated that those adsorbates were clearly adsorbed on AB- $\text{Fe}_3\text{O}_4$  in this system.



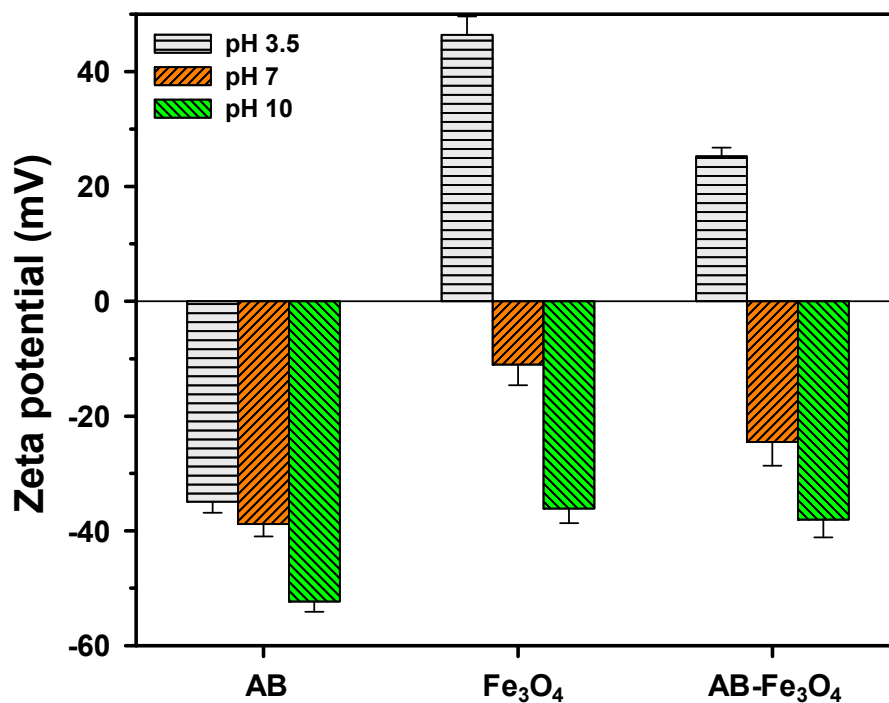
**Figure 2.** FTIR spectra of (a) biochar, AB, Fe<sub>3</sub>O<sub>4</sub>, and AB-Fe<sub>3</sub>O<sub>4</sub> and (b) AB-Fe<sub>3</sub>O<sub>4</sub> before and after TeCP, TCP, and DCP adsorption.

Figure 3a–c shows representative SEM images and EDX spectra of AB, Fe<sub>3</sub>O<sub>4</sub>, and AB-Fe<sub>3</sub>O<sub>4</sub>, respectively. SEM images revealed that both AB and Fe<sub>3</sub>O<sub>4</sub> were spherical in shape, measuring 10–100  $\mu$ m (Figure 3a,c) and ~20 nm (Figure 3b) in diameter, respectively. Using EDX (Figure 3a,b), we determined that the main elements of AB and Fe<sub>3</sub>O<sub>4</sub> were C/O and O/Fe, respectively. The basis for our conclusion of the composite of AB-Fe<sub>3</sub>O<sub>4</sub>—as shown in Figure 3c—is as follows: (a) Fe<sub>3</sub>O<sub>4</sub> nanoparticles uniformly covered AB surface through SEM image, and (b) elements of C (55 wt%), O (20 wt%), and Fe (25 wt%) were detected through EDX analysis.



**Figure 3.** Representative SEM images and energy-dispersive x-ray spectroscopy (EDX) spectra of (a) AB, (b)  $\text{Fe}_3\text{O}_4$ , and (c) AB- $\text{Fe}_3\text{O}_4$ .

We measured the surface charge of AB,  $\text{Fe}_3\text{O}_4$ , and AB- $\text{Fe}_3\text{O}_4$  at pH 3.5, 7, and 10, as shown in Figure 4. The isoelectric points of AB and AB- $\text{Fe}_3\text{O}_4$  were lower and higher than pH 3.5, respectively, meaning that AB- $\text{Fe}_3\text{O}_4$  had a much higher positive surface charge than AB due to the positive surface charge of  $\text{Fe}_3\text{O}_4$  at pH 3.5. Thus, we concluded that AB- $\text{Fe}_3\text{O}_4$  was able to achieve better adsorption capacity than AB if adsorbates were at a negative surface charge and a weak acid condition. Increased isoelectric point after composition with  $\text{Fe}_3\text{O}_4$  was consistent with other studies, because the pH of zero point charge of  $\text{Fe}_3\text{O}_4$  was close to pH 5–6 [39].



**Figure 4.** Variations in the surface (zeta) potential of AB,  $\text{Fe}_3\text{O}_4$ , and AB- $\text{Fe}_3\text{O}_4$  with solution pH (pH 3.5, 7, and 10) at 298 K. Error bars indicate the standard deviations for at least triplicate measurements.

We analyzed the paramagnetic property of  $\text{Fe}_3\text{O}_4$  and AB- $\text{Fe}_3\text{O}_4$  using magnetic hysteresis loops, as shown in Figure 5. The magnetization curves of  $\text{Fe}_3\text{O}_4$  and AB- $\text{Fe}_3\text{O}_4$  showed that the specific saturation magnetizations of  $\text{Fe}_3\text{O}_4$  and AB- $\text{Fe}_3\text{O}_4$  were 85.6 and 13.3 emu/g, respectively. The lower saturation value of AB- $\text{Fe}_3\text{O}_4$  compared to that of  $\text{Fe}_3\text{O}_4$  could have been the result of lower  $\text{Fe}_3\text{O}_4$  content in the AB- $\text{Fe}_3\text{O}_4$  composite [40]. The specific saturation magnetization of  $\text{Fe}_3\text{O}_4$  was comparable to a previous report (e.g., approximately 80 emu/g [39]). Thus, the used AB- $\text{Fe}_3\text{O}_4$  adsorbent could be easily separated and recycled via external magnetic fields based on specific saturation magnetization of AB- $\text{Fe}_3\text{O}_4$ .

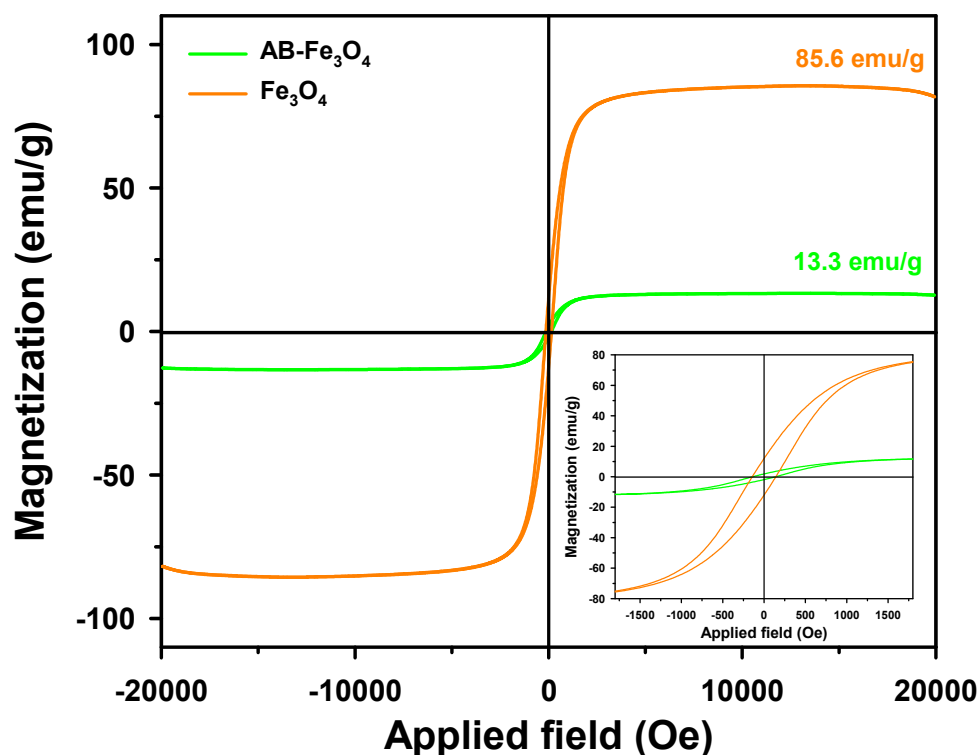


Figure 5. Room temperature magnetic hysteresis loops of  $\text{Fe}_3\text{O}_4$  and  $\text{AB-Fe}_3\text{O}_4$ .

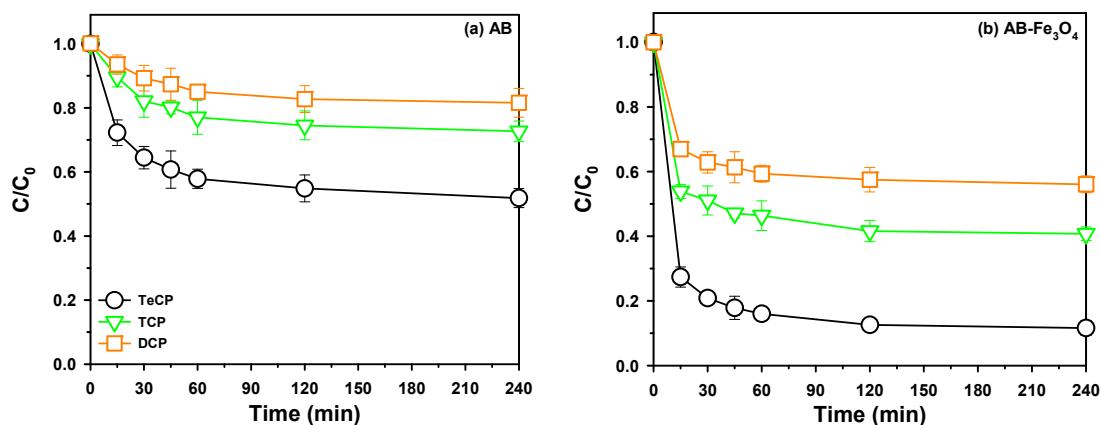
Physical properties of AB,  $\text{Fe}_3\text{O}_4$ , and  $\text{AB-Fe}_3\text{O}_4$  were confirmed by porosimeter, and Table 2 summarizes specific surface area and total pore volume. Two physical properties of  $\text{AB-Fe}_3\text{O}_4$  were improved from  $2.06 \text{ m}^2/\text{g}$  and  $6.13 \times 10^{-3} \text{ cm}^3/\text{g}$  to  $2.89 \text{ m}^2/\text{g}$  and  $1.43 \times 10^{-2} \text{ cm}^3/\text{g}$  in the case of specific surface area and total pore volume, respectively, after the introduction of  $\text{Fe}_3\text{O}_4$ . Hence, composition with  $\text{Fe}_3\text{O}_4$  had merit for its higher adsorption sites if van der Waals force was a major mechanism between adsorbent and adsorbate [41]. After having evaluated all adsorption performances under several experimental parameters, we describe each adsorption mechanism in the following sections.

Table 2. Textural characteristics of AB,  $\text{Fe}_3\text{O}_4$ , and  $\text{AB-Fe}_3\text{O}_4$ .

Sample	AB	$\text{Fe}_3\text{O}_4$	$\text{AB-Fe}_3\text{O}_4$
Specific surface area ( $\text{m}^2/\text{g}$ )	2.06	9.29	2.89
Total pore volume ( $\text{cm}^3/\text{g}$ )	$6.13 \times 10^{-3}$	$5.58 \times 10^{-1}$	$1.43 \times 10^{-2}$

### 3.2. Effect of Contact Time on Polychlorophenols Adsorption and Investigation of its Mechanism

It was important to determine the contact time for equilibrium state in the adsorption process from an engineering perspective. We measured the effect of contact time on the uptake of TeCP, TCP, and DCP on AB and  $\text{AB-Fe}_3\text{O}_4$ , as shown in Figure 6a,b, respectively. Both adsorbents showed that adsorption performances of TeCP, TCP, and DCP reached an equilibrium state within 60 min. Two kinetic models were applied to investigate kinetic studies of AB and  $\text{AB-Fe}_3\text{O}_4$  on adsorption of TeCP, TCP, and DCP. Table 3 summarizes kinetic parameters of TeCP, TCP, and DCP adsorption by AB and  $\text{AB-Fe}_3\text{O}_4$ . The pseudo-second-order kinetic model was better suited for explaining the kinetic adsorption efficiency of both adsorbents, thus chemisorption was the main kinetic mechanism of this system [15]. These results were consistent with other research [12,25], which reported carbon-based materials as the adsorbent for removal of DCP.



**Figure 6.** Effect of contact time on the uptake of TeCP, TCP, and DCP on (a) AB and (b) AB-Fe<sub>3</sub>O<sub>4</sub> at pH 3.5 ( $C_0 = 5$  mg/L,  $V = 30$  mL, adsorbent mass 30 mg, and agitation speed = 300 rpm).  $C$  indicates the remaining concentration of TeCP, TCP, and DCP in the solution at time  $t$ .

**Table 3.** Kinetic parameters of TeCP, TCP, and DCP adsorption by AB and AB-Fe<sub>3</sub>O<sub>4</sub>.

Adsorbate /Adsorbent	TeCP /AB	TCP /AB	DCP /AB	TeCP /AB-Fe <sub>3</sub> O <sub>4</sub>	TCP /AB-Fe <sub>3</sub> O <sub>4</sub>	DCP /AB-Fe <sub>3</sub> O <sub>4</sub>
<b>Pseudo-first-order</b>						
$q_e$ (mg/g)	1.0743	1.0730	1.0278	1.0668	1.0857	1.6195
$k_1$ (min <sup>-1</sup> )	0.0174	0.0202	0.0221	0.0261	0.0260	0.0188
$R^2$	0.9417	0.9586	0.9874	0.9968	0.9848	0.9676
<b>Pseudo-second-order</b>						
$q_e$ (mg/g)	2.4820	1.5649	1.1216	4.5126	3.0600	2.2242
$k_2$ (g mg <sup>-1</sup> min <sup>-1</sup> )	0.0346	0.0250	0.0262	0.0535	0.0483	0.0769
$R^2$	0.9998	0.9929	0.9951	0.9999	0.9988	0.9998

Furthermore, Figure 6a,b shows that performance in the removal of polychlorophenols from the aqueous solutions by using AB and AB-Fe<sub>3</sub>O<sub>4</sub> was ranked in the following order: DCP < TCP < TeCP. This phenomenon could be explained by the following adsorption mechanisms, as concluded in previous studies [12]: (a) hydrogen bonding (H-bond), (b) electrostatic interactions, (c) hydrophobic interactions, and (d) non-covalent  $\pi$ -electron acceptor–donor interactions.

H-bond between adsorbent and adsorbate is a useful factor in determining adsorption mechanisms. In this system, all three adsorbates include one hydroxyl group, thus they can act as both a hydrogen acceptor and a donor, and the number of hydrogen acceptors or donors is a critical factor in controlling adsorption performances. Thus, if H-bond was a major adsorption mechanism, adsorption performances should have been similar, regardless of the role of adsorbates for H-bond, based on only one hydroxyl group. However, TeCP was removed much more efficiently by both adsorbents as compared to TCP and DCP, which suggested that H-bond may not have been the most significant. Other factors would have affected the sorption process.

Electrostatic interactions are good parameters for identifying adsorption mechanisms, because they are easily confirmed by the characteristics of surface charge between adsorbent and adsorbate. Based on  $pK_a$  of TeCP (5.22), TCP (6.23), and DCP (7.89), as shown in Table 1, they existed in a neutral state at pH 3.5, which is the experimental condition depicted in Figure 6a,b. Hence, if electrostatic interactions were a critical adsorption mechanism, adsorption performances should have been consistent, irrespective of the surface charge of adsorbents, considering the neutral state of adsorbates at pH 3.5. Therefore, electrostatic interactions were not the most likely explanation for the adsorption

mechanism in this system, considering TeCP's removal rate was the highest compared to TCP and DCP.

Hydrophobic interactions are a significant factor when the target compounds have high hydrophobic characteristics. Table 1 shows the water solubility of TeCP, TCP, and DCP, which could be used as representative parameters for the degree of hydrophobicity of adsorbates. That is, hydrophobicity of adsorbates existed in the following order: TeCP > TCP > DCP. This order was the exact pattern of removal rate of the adsorbates shown in Figure 6a,b. The results of previous studies also concluded that hydrophobic organic pollutants were efficiently treated by biochar via hydrophobic interactions [23]; therefore, hydrophobic interaction was one of the important roles in the removal of the target contaminants.

According to another study [12], non-covalent  $\pi$ -electron acceptor–donor interactions were a major adsorption mechanism for removing DCP by biochar. Thus, we applied this adsorption mechanism to our system. A major difference in the chemical structure of TeCP, TCP, and DCP is the number of chlorides, which plays a role as the electron-withdrawn atom [12]. In other words, the electron density of a benzene ring of adsorbates continuously decreases as the number of attached chloride atoms increases. Meanwhile, biochar contains a lot of oxygenated functional groups after activation that act as electron-donors. Therefore, non-covalent  $\pi$ -electron acceptor–donor interactions could be a reasonable explanation for the adsorption mechanism in this system. This was particularly revealed by the deficient electron density atmosphere of TeCP, because the intrinsic molecular structure of TeCP contains the highest number of chloride atoms.

Subsequently, adsorption performances of AB-Fe<sub>3</sub>O<sub>4</sub> were better than AB (Figure 6a,b), and these results could be explained by (a) stronger non-covalent  $\pi$ -electron acceptor–donor interactions attributed to higher oxygen content as an electron-donor group [12] and (b) larger surface area judging by the results from the porosimeter (Table 2). Considering TeCP's high removal efficiency rate, we thoroughly investigate its use as an adsorbate in following sections.

### 3.3. Effect of Solution pH and Initial TeCP Concentration on TeCP Adsorption Performances

Surface charge of both adsorbents and adsorbates is attributed to solution pH; thus, we tested the effect of solution pH on the uptake of TeCP by AB and AB-Fe<sub>3</sub>O<sub>4</sub> (Figure 7). Both adsorbents showed that adsorption performances were almost constant in the range of pH 3–9. In the case of AB, adsorption rates at neutral and basic conditions were lower than acidic conditions, thus electrostatic repulsion acted as a supplementary effect in this system considering its higher negative surface charge than AB-Fe<sub>3</sub>O<sub>4</sub> (Figure 4) and pK<sub>a</sub> of TeCP (Table 1). Furthermore, we measured the initial and the final pH, as described in Figure 4, and both adsorbents showed that the initial pH was higher than the final pH at over pH 5. This phenomenon might have been attributed to the reaction between ionized TeCP and hydroxyl ion in the solution [42].

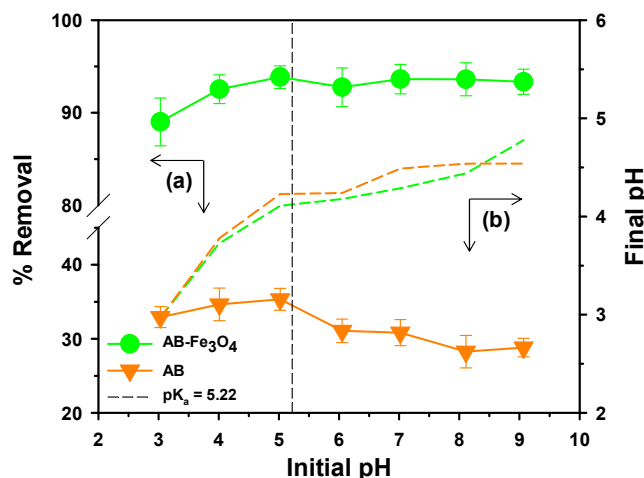


**Figure 7.** (a) Effect of solution pH on the uptake of TeCP by AB and AB-Fe<sub>3</sub>O<sub>4</sub> ( $C_0 = 5$  mg/L,  $V = 30$  mL, adsorbent mass 30 mg, agitation speed = 300 rpm, temperature =  $25 \pm 1^\circ\text{C}$ , and reaction time = 120 min); and (b) the final pH of the solution.

The effect of the initial TeCP concentration with a different contact time on TeCP adsorption was evaluated by AB and AB-Fe<sub>3</sub>O<sub>4</sub>, as shown in Figure 8a,b, respectively. As mentioned above, the removal rate of TeCP by AB-Fe<sub>3</sub>O<sub>4</sub> was higher than AB, regardless of the initial concentration of TeCP, due to stronger non-covalent  $\pi$ -electron acceptor–donor interactions and larger surface area. Furthermore, the removal rate of TeCP continuously decreased with the increasing initial concentration of TeCP in both AB and AB-Fe<sub>3</sub>O<sub>4</sub> cases, and these results could be explained by the fact that limited active sites were available when the mass of the adsorbent was fixed for binding adsorbates [43].

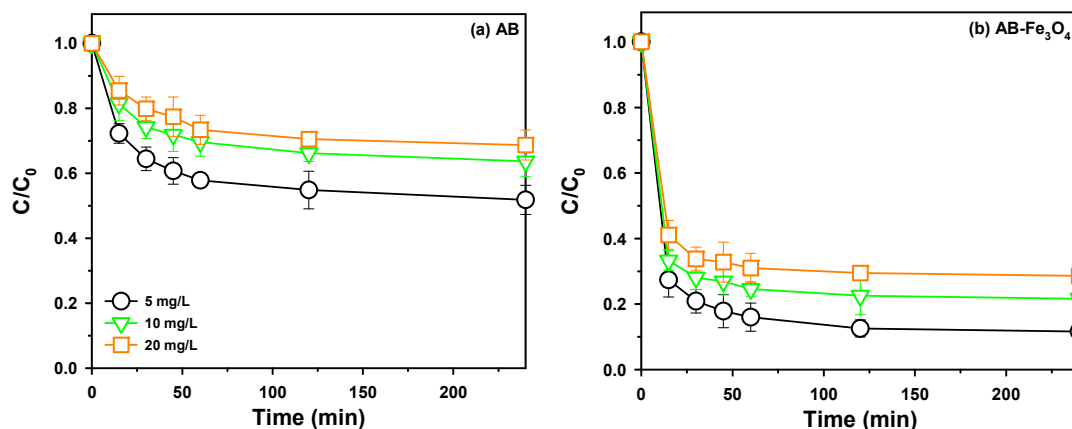


**Figure 8.** Effect of initial TeCP concentration and contact time on adsorption of TeCP by (a) AB and (b) AB-Fe<sub>3</sub>O<sub>4</sub> at pH 3.5 ( $V = 30$  mL, adsorbent mass 30 mg, agitation speed = 300 rpm, temperature =  $25 \pm 1^\circ\text{C}$ , and reaction time = 120 min).

Subsequently, we tried to evaluate equilibrium isotherms for adsorption of TeCP on AB and AB-Fe<sub>3</sub>O<sub>4</sub> for further investigation. In this study, we employed the Langmuir and the Freundlich isotherm models to correlate the adsorption capacities and the residual concentrations of TeCP left in the aqueous solutions [15]. Figure 9 describes the effect of initial concentration of adsorbates (i.e., 5, 10, 20, 60, 100, and 200 mg/L) on adsorption capacity ( $q_e$ ), and two isotherm models were plotted using the  $q_e$  results. Freundlich isotherm better explained the equilibrium of TeCP adsorption on both AB and AB-Fe<sub>3</sub>O<sub>4</sub> cases based on the higher correlation coefficients ( $R^2$ ,  $R^2$  of AB and AB-Fe<sub>3</sub>O<sub>4</sub> of Langmuir/Freundlich isotherm models were 0.9368/0.9653 and 0.8724/0.9974, respectively). This result was similar to previous studies [12,25], which reported biochar and activated charcoal as adsorbents for DCP treatment in aqueous phase.

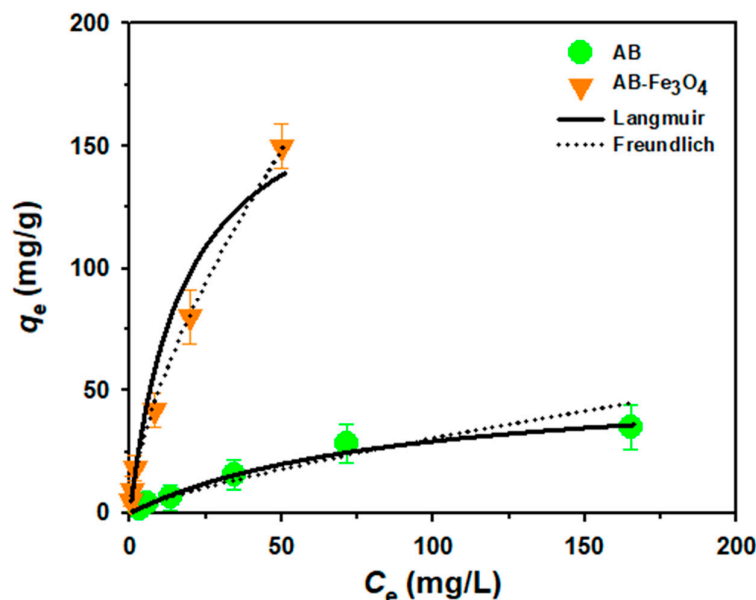


**Figure 9.** Equilibrium isotherms for adsorption of TeCP on AB and AB-Fe<sub>3</sub>O<sub>4</sub> at pH 3.5 ( $V = 30$  mL, adsorbent mass 30 mg, agitation speed = 300 rpm, temperature =  $25 \pm 1^\circ\text{C}$ , and reaction time = 240 min).

### 3.4. Adsorption Selectivity for TeCP over BPA and SMX

From a practical perspective, adsorption selectivity for TeCP over other organic pollutants is an important parameter, and BPA and SMX were chosen as representative organic pollutants because they have been commonly detected in a wastewater effluent [44]. Figure 10a,b describes the effect of contact time on the uptake of TeCP with the presence of BPA and SMX, respectively. The removal rate of TeCP was better compared to that of BPA and SMX, thus AB-Fe<sub>3</sub>O<sub>4</sub> could be used as a novel adsorbent for the selective removal of TeCP in wastewater. To conduct further investigation, we referred to a previous method and calculated the mixture selectivity between two different adsorbates by each concentration ratio in the feed solution [45]. Mixture selectivities at 240 min in the case of TeCP/BPA (Figure 10a) and TeCP/SMX (Figure 10b) were 2.31 and 11.14, respectively. These results could be attributed to the hydrophobic interactions because TeCP has a higher number of hydrophobic characteristics than BPA and SMX considering  $\log K_{ow}$  of TeCP (4.45), BPA (3.32), and SMX (0.89), as shown in Table 1. Thus, these results also suggested that hydrophobic interactions played a role as the main adsorption mechanism in this study, and AB-Fe<sub>3</sub>O<sub>4</sub> could be applied to the selective removal of TeCP in wastewater judging from its high adsorption selectivity (Figure 10a,b). Table 4 summarizes the comparison of polychlorinated compounds removal by reported adsorbents in the literature and this study. AB-Fe<sub>3</sub>O<sub>4</sub> showed comparable or higher adsorption performances compared to the previously reported adsorbents.

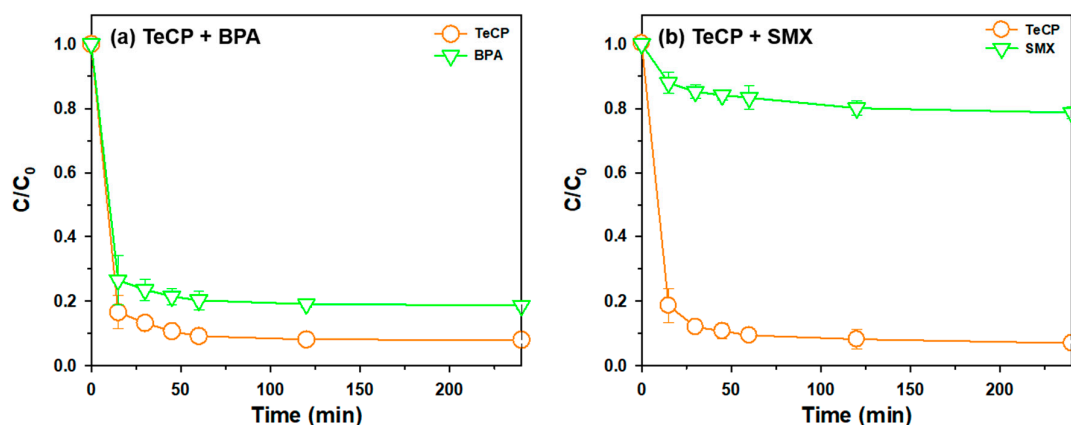


**Figure 10.** Effect of contact time on the uptake of TeCP with the presence of (a) BPA and (b) SMX on AB-Fe<sub>3</sub>O<sub>4</sub> at pH 3.5 ( $C_0 = 5$  mg/L,  $V = 30$  mL, adsorbent mass 30 mg, temperature =  $25 \pm 1^\circ\text{C}$ , and agitation speed = 300 rpm).

**Table 4.** Comparison of polychlorinated compounds removal by reported adsorbents in the literature and this study.

Adsorbent	Polychlorinated compounds	Experimental conditions	$q_{\max}$ (mg/g)	Reference
Cattail fiber-based activated carbon	DCP	200 mg/L adsorbate using 100 mg/L adsorbent	142.8	[42]
Oil palm empty fruit bunch carbon	DCP	250 mg/L adsorbate using 5 mg/L adsorbent	27.3	[46]
Palm pith carbon	DCP	40 mg/L adsorbate using 2,000 mg/L adsorbent	19.2	[47]
Coconut shell-based activated carbon	TCP	100 mg/L adsorbate using 5,000 mg/L adsorbent	122.3	[48]
Activated carbon	TCP	100 mg/L adsorbate using 5,000 mg/L adsorbent	112.4	[48]
AB	TeCP	200 mg/L adsorbate using 1,000 mg/L adsorbent	34.8	This study
AB-Fe <sub>3</sub> O <sub>4</sub>	TeCP	200 mg/L adsorbate using 1,000 mg/L adsorbent	149.8	This study

#### 4. Conclusions

In this study, we characterized biochar, AB, Fe<sub>3</sub>O<sub>4</sub>, and AB-Fe<sub>3</sub>O<sub>4</sub> via PXRD, FTIR, SEM-EDX, zeta potential analyzer, VSM, and porosimeter. These characterizations revealed successful synthesis of AB-Fe<sub>3</sub>O<sub>4</sub> composite, which was utilized as a novel adsorbent to remove polychlorophenols (TeCP, TCP, and DCP). Furthermore, the results of the kinetic and the isotherm experiments obtained in this study were well matched to the pseudo-second-order kinetic model and the Freundlich isotherm model, respectively. The chemisorption of polychlorophenols on AB-Fe<sub>3</sub>O<sub>4</sub> in this system was verified by FTIR spectra analysis before and after adsorption. Major adsorption mechanisms of this system

were attributed to both hydrophobic interactions and non-covalent  $\pi$ -electron acceptor–donor interactions judging by the intrinsic properties of polychlorophenols and adsorbents. Lastly, we measured adsorption selectivity for TeCP over other organic pollutants (i.e., BPA and SMX) because it is an important factor from a practical perspective. Removal rate of TeCP was outstanding compared to BPA and SMX due to hydrophobic interactions; thus, we conclude that AB-Fe<sub>3</sub>O<sub>4</sub> can be applied in the selective removal of TeCP in wastewater based on its results of high selectivity.

**Author Contributions:** C. M. Park and Y. Kim designed and carried out this research. J. Han and Y. Yoon supervised and instructed this research. B.-M. Jun wrote this paper. J. Kim prepared and analyzed the data. C. M. Park provided advices and help in this paper revision. All authors have approved the manuscript.

**Funding:** This study was supported by the Basic Science Research Program through the National Research Foundation of Korea (NRF) funded by the Ministry of Education (NRF-2018R1A6A1A03024962), and the Korea Ministry of Environment (The SEM projects; 2018002470005).

**Conflicts of Interest:** The authors declare no conflict of interest.

**Acknowledgments:** The authors are grateful to the anonymous reviewers for their insightful and constructive comments, which greatly improved the quality of the paper.

## References

- Demey, H.; Tria, S.A.; Soleri, R.; Guiseppi-Elie, A.; Bazin, I. Sorption of his-tagged Protein G and Protein G onto chitosan/divalent metal ion sorbent used for detection of microcystin-LR. *Environ. Sci. Pollut. R.* **2017**, *24*, 15–24.
- Han, S.-W.; Kim, W.; Lee, Y.; Jun, B.-M.; Kwon, Y.-N. Investigation of Hydrate-induced Ice Desalination (HIID) and its application to a pretreatment of reverse osmosis (RO) process. *Desalination* **2016**, *395*, 8–16.
- Attar, K.; Bouazza, D.; Miloudi, H.; Tayeb, A.; Boos, A.; Sastre, A.M.; Demey, H. Cadmium removal by a low-cost magadiite-based material: Characterization and sorption applications. *J. Environ. Chem. Eng.* **2018**, *6*, 5351–5360.
- Jun, B.-M.; Nguyen, T.P.N.; Kim, Y.-K.; Lee, H.K.; Kwon, Y.-N. Surface modification of TFC FO membrane using N-isopropylacrylamide (NIPAM) to enhance fouling resistance and cleaning efficiency. *Desalin. Water Treat.* **2017**, *65*, 11–21.
- Demey, H.; Melkior, T.; Chatroux, A.; Attar, K.; Thiery, S.; Miller, H.; Grateau, M.; Sastre, A.M.; Marchand, M. Evaluation of torrefied poplar-biomass as a low-cost sorbent for lead and terbium removal from aqueous solutions and energy co-generation. *Chem. Eng. J.* **2019**, *361*, 839–852.
- Fernández-Castro, P.; San Román, M.F.; Ortiz, I. Theoretical and experimental formation of low chlorinated dibenzo-p-dioxins and dibenzofurans in the Fenton oxidation of chlorophenol solutions. *Chemosphere* **2016**, *161*, 136–144.
- Choi, J.-H.; Kim, Y.-H. Reduction of 2,4,6-trichlorophenol with zero-valent zinc and catalyzed zinc. *J. Hazard. Mater.* **2009**, *166*, 984–991.
- Schmid, P.; Bogdal, C.; Wang, Z.; Azara, V.; Haag, R.; von Arx, U. Releases of chlorobenzenes, chlorophenols and dioxins during fireworks. *Chemosphere* **2014**, *114*, 158–164.
- Chen, M.-L.; Min, J.-Q.; Pan, S.-D.; Jin, M.-C. Surface core-shell magnetic polymer modified graphene oxide-based material for 2,4,6-trichlorophenol removal. *RSC Adv.* **2014**, *4*, 63494–63501.
- Xiong, Z.; Xu, Y.; Zhu, L.; Zhao, J. Enhanced photodegradation of 2,4,6-trichlorophenol over palladium phthalocyaninesulfonate modified organobentonite. *Langmuir* **2005**, *21*, 10602–10607.
- Liu, Q.-S.; Zheng, T.; Wang, P.; Jiang, J.-P.; Li, N. Adsorption isotherm, kinetic and mechanism studies of some substituted phenols on activated carbon fibers. *Chem. Eng. J.* **2010**, *157*, 348–356.
- Kalderis, D.; Kayan, B.; Akay, S.; Kulaksız, E.; Gözmen, B. Adsorption of 2,4-dichlorophenol on paper sludge/wheat husk biochar: Process optimization and comparison with biochars prepared from wood chips, sewage sludge and hog fuel/demolition waste. *J. Environ. Chem. Eng.* **2017**, *5*, 2222–2231.
- Wang, C.C.; Lee, C.M.; Lu, C.J.; Chuang, M.S.; Huang, C.Z. Biodegradation of 2,4,6-trichlorophenol in the presence of primary substrate by immobilized pure culture bacteria. *Chemosphere* **2000**, *41*, 1873–1879.
- Eker, S.; Kargi, F. Biological treatment of 2,4,6-trichlorophenol (TCP) containing wastewater in a hybrid bioreactor system with effluent recycle. *J. Environ. Manag.* **2009**, *90*, 692–698.

15. Jun, B.-M.; Kim, S.; Kim, Y.; Her, N.; Heo, J.; Han, J.; Jang, M.; Park, C.M.; Yoon, Y. Comprehensive evaluation on removal of lead by graphene oxide and metal organic framework. *Chemosphere* **2019**, *231*, 82–92.
16. Han, J.; Jun, B.-M.; Heo, J.; Lee, G.; Yoon, Y.; Park, C.M. Highly efficient organic dye removal from waters by magnetically recoverable  $\text{La}_2\text{O}_3/\text{ZnFe}_2\text{O}_4$ -reduced graphene oxide nanohybrid. *Ceram. Int.* **2019**, *45*, 19247–19256.
17. Park, C.M.; Kim, Y.M.; Kim, K.-H.; Wang, D.; Su, C.; Yoon, Y. Potential utility of graphene-based nano spinel ferrites as adsorbent and photocatalyst for removing organic/inorganic contaminants from aqueous solutions: A mini review. *Chemosphere* **2019**, *221*, 392–402.
18. Su, C. Environmental implications and applications of engineered nanoscale magnetite and its hybrid nanocomposites: A review of recent literature. *J. Hazard. Mater.* **2017**, *322*, 48–84.
19. Maziarz, P.; Matusik, J.; Leiviskä, T.; Strączek, T.; Kapusta, C.; Marek Woch, W.; Tokarz, W.; Górniak, K. Toward highly effective and easily separable halloysite-containing adsorbents: The effect of iron oxide particles impregnation and new insight into As(V) removal mechanisms. *Sep. Purif. Technol.* **2019**, *210*, 390–401.
20. Maziarz, P.; Matusik, J.; Strączek, T.; Kapusta, C.; Woch, W.M.; Tokarz, W.; Radziszewska, A.; Leiviskä, T. Highly effective magnet-responsive LDH-Fe oxide composite adsorbents for As(V) removal. *Chem. Eng. J.* **2019**, *362*, 207–216.
21. Zhou, Y.; Gao, B.; Zimmerman, A.R.; Chen, H.; Zhang, M.; Cao, X. Biochar-supported zerovalent iron for removal of various contaminants from aqueous solutions. *Bioresour. Technol.* **2014**, *152*, 538–542.
22. Devi, P.; Saroha, A.K. Simultaneous adsorption and dechlorination of pentachlorophenol from effluent by Ni-ZVI magnetic biochar composites synthesized from paper mill sludge. *Chem. Eng. J.* **2015**, *271*, 195–203.
23. Tan, X.-F.; Liu, S.-B.; Liu, Y.-G.; Gu, Y.-L.; Zeng, G.-M.; Hu, X.-J.; Wang, X.; Liu, S.-H.; Jiang, L.-H. Biochar as potential sustainable precursors for activated carbon production: Multiple applications in environmental protection and energy storage. *Bioresour. Technol.* **2017**, *227*, 359–372.
24. Wang, Z.; Wu, J.; He, T.; Wu, J. Corn stalks char from fast pyrolysis as precursor material for preparation of activated carbon in fluidized bed reactor. *Bioresour. Technol.* **2014**, *167*, 551–554.
25. Ma, J.-W.; Wang, H.; Wang, F.-Y.; Huang, Z.-H. Adsorption of 2,4-dichlorophenol from aqueous solution by a new low-cost adsorbent—Activated bamboo charcoal. *Sep. Sci. Technol.* **2010**, *45*, 2329–2336.
26. Park, C.M.; Heo, J.; Wang, D.; Su, C.; Yoon, Y. Heterogeneous activation of persulfate by reduced graphene oxide–elemental silver/magnetite nanohybrids for the oxidative degradation of pharmaceuticals and endocrine disrupting compounds in water. *Appl. Catal. B* **2018**, *225*, 91–99.
27. Janoš, P.; Kormunda, M.; Životský, O.; Pilařová, V. Composite  $\text{Fe}_3\text{O}_4$ /humic acid magnetic sorbent and its sorption ability for chlorophenols and some other aromatic compounds. *Sep. Sci. Technol.* **2013**, *48*, 2028–2035.
28. Jiang, W.; Cai, Q.; Xu, W.; Yang, M.; Cai, Y.; Dionysiou, D.D.; O’Shea, K.E. Cr(VI) adsorption and reduction by humic acid coated on magnetite. *Environ. Sci. Technol.* **2014**, *48*, 8078–8085.
29. Qian, L.; Chen, B. Interactions of aluminum with biochars and oxidized biochars: Implications for the biochar aging process. *J. Agric. Food Chem.* **2014**, *62*, 373–380.
30. Wang, Z.; Guo, H.; Yu, Y.; He, N. Synthesis and characterization of a novel magnetic carrier with its composition of  $\text{Fe}_3\text{O}_4$ /carbon using hydrothermal reaction. *J. Magn. Magn. Mater.* **2006**, *302*, 397–404.
31. Liu, H.; Ruan, X.; Zhao, D.; Fan, X.; Feng, T. Enhanced adsorption of 2,4-dichlorophenol by nanoscale zero-valent iron loaded on bentonite and modified with a cationic surfactant. *Ind. Eng. Chem. Res.* **2017**, *56*, 191–197.
32. Khenifi, A.; Zohra, B.; Kahina, B.; Houari, H.; Zoubir, D. Removal of 2,4-DCP from wastewater by CTAB/bentonite using one-step and two-step methods: A comparative study. *Chem. Eng. J.* **2009**, *146*, 345–354.
33. Jun, B.-M.; Kim, S.H.; Kwak, S.K.; Kwon, Y.-N. Effect of acidic aqueous solution on chemical and physical properties of polyamide NF membranes. *Appl. Surf. Sci.* **2018**, *444*, 387–398.
34. Wang, L.; Gan, K.; Lu, D.; Zhang, J. Hydrophilic  $\text{Fe}_3\text{O}_4$ @C for high-capacity adsorption of 2,4-dichlorophenol. *Eur. J. Inorg. Chem.* **2016**, *2016*, 890–896.
35. Hadjittofi, L.; Prodromou, M.; Pashalidis, I. Activated biochar derived from cactus fibres—Preparation, characterization and application on Cu(II) removal from aqueous solutions. *Bioresour. Technol.* **2014**, *159*, 460–464.

36. Dik, P.P.; Klimov, O.V.; Danilova, I.G.; Leonova, K.A.; Pereyma, V.Y.; Budukva, S.V.; Uvarkina, D.D.; Kazakov, M.O.; Noskov, A.S. Hydroprocessing of hydrocracker bottom on Pd containing bifunctional catalysts. *Catal. Today* **2016**, *271*, 154–162.
37. Pei, Z.; Li, L.; Sun, L.; Zhang, S.; Shan, X.-Q.; Yang, S.; Wen, B. Adsorption characteristics of 1,2,4-trichlorobenzene, 2,4,6-trichlorophenol, 2-naphthol and naphthalene on graphene and graphene oxide. *Carbon* **2013**, *51*, 156–163.
38. Fan, J.; Zhang, J.; Zhang, C.; Ren, L.; Shi, Q. Adsorption of 2,4,6-trichlorophenol from aqueous solution onto activated carbon derived from *loosestrife*. *Desalination* **2011**, *267*, 139–146.
39. Liu, J.-F.; Zhao, Z.-S.; Jiang, G.-B. Coating Fe<sub>3</sub>O<sub>4</sub> magnetic nanoparticles with humic acid for high efficient removal of heavy metals in water. *Environ. Sci. Technol.* **2008**, *42*, 6949–6954.
40. Huang, J.; Chang, Q.; Ding, Y.; Han, X.; Tang, H. Catalytic oxidative removal of 2,4-dichlorophenol by simultaneous use of horseradish peroxidase and graphene oxide/Fe<sub>3</sub>O<sub>4</sub> as catalyst. *Chem. Eng. J.* **2014**, *254*, 434–442.
41. Hasan, Z.; Jhung, S.H. Removal of hazardous organics from water using metal-organic frameworks (MOFs): Plausible mechanisms for selective adsorptions. *J. Hazard. Mater.* **2015**, *283*, 329–339.
42. Ren, L.; Zhang, J.; Li, Y.; Zhang, C. Preparation and evaluation of cattail fiber-based activated carbon for 2,4-dichlorophenol and 2,4,6-trichlorophenol removal. *Chem. Eng. J.* **2011**, *168*, 553–561.
43. Joseph, L.; Jun, B.-M.; Jang, M.; Park, C.M.; Muñoz-Senmache, J.C.; Hernández-Maldonado, A.J.; Heyden, A.; Yu, M.; Yoon, Y. Removal of contaminants of emerging concern by metal-organic framework nano-adsorbents: A review. *Chem. Eng. J.* **2019**, *369*, 928–946.
44. Heo, J.; Yoon, Y.; Lee, G.; Kim, Y.; Han, J.; Park, C.M. Enhanced adsorption of bisphenol A and sulfamethoxazole by a novel magnetic CuZnFe<sub>2</sub>O<sub>4</sub>-biochar composite. *Bioresour. Technol.* **2019**, *281*, 179–187.
45. Jun, B.-M.; Lee, H.K.; Kwon, Y.-N. Acid-catalyzed hydrolysis of semi-aromatic polyamide NF membrane and its application to water softening and antibiotics enrichment. *Chem. Eng. J.* **2018**, *332*, 419–430.
46. Alam, Z.; Muyibi, S.A.; Toramae, J. Statistical optimization of adsorption processes for removal of 2,4-dichlorophenol by activated carbon derived from oil palm empty fruit bunches. *J. Environ. Sci.* **2007**, *19*, 674–677.
47. Sathishkumar, M.; Binupriya, A.R.; Kavitha, D.; Yun, S.E. Kinetic and isothermal studies on liquid-phase adsorption of 2,4-dichlorophenol by palm pith carbon. *Bioresour. Technol.* **2007**, *98*, 866–873.
48. Radhika, M.; Palanivelu, K. Adsorptive removal of chlorophenols from aqueous solution by low cost adsorbent—Kinetics and isotherm analysis. *J. Hazard. Mater.* **2006**, *138*, 116–124.

